Numerical Simulation of Supersonic and Hypersonic Turbulent Compression Corner Flows

C. M. Hung* and R. W. MacCormack†
NASA Ames Research Center, Moffett Field, Calif.

A relaxation turbulence eddy viscosity model is incorporated to solve the complete Navier-Stokes equations for supersonic and hypersonic flows over a two-dimensional compression corner. The system of equations is solved by a time-split, second-order accurate numerical scheme. Details of the relaxation process are studied. In general, using the relaxation model, the eddy viscosity value in the outer layer of the separation region is reduced substantially, and good improvement in the prediction of upstream pressure propagation is obtained for a Mach number of 2.96 and Reynolds number of 10^7, with wedge angle of 25°. However, the application of the relaxation model to hypersonic flow at Mach number 8.66 and Reynolds number of 22×10^6, with highly cooled wall, shows unfavorable effects on heat transfer and skin friction in the reattachment and recompression regions.

Introduction

WITH the advent of large high-speed computers and efficient numerical schemes, increased interest has been given recently to the numerical simulation of compressible flows with strong viscous and inviscid interactions. One such problem, which has received considerable attention, is supersonic or hypersonic flow over a two-dimensional compression corner. The large adverse pressure gradient generated by the wedge leads to boundary-layer separation, and the flowfield is characterized by the complicated interaction of the viscous dominated region adjacent to the wall with the outer inviscid stream.

Previous theoretical approaches to solve this problem usually have been made with the boundary-layer equations. Such an approach, in general, encounters the question of uniqueness, because both the initial condition and the "jump" conditions from supercritical to subcritical type of boundary layers cannot be specified completely *a priori*. Use of the complete Navier-Stokes equations, which recently has attracted much attention (see extensive review of Ref. 1), overcomes this question and removes the often employed restrictive assumption that the static pressure is constant across the boundary layer.

Numerical solutions of Navier-Stokes equations for laminar flow cases[2-4] have produced results in close agreement with experimental measurements. However, the extension to the complete Reynolds averaged Navier-Stokes equations for turbulent flow has not produced convincing results yet, although it is currently attracting a great deal of interest. One of the major difficulties, other than computer and numerical technique limitations, is the lack of an accurate model. Turbulence model development is the pacing item for viscous flowfield simulation.

In viscous and inviscid interactions, turbulence is out of equilibrium. The idea of nonequilibrium turbulence was realized by Jacobs[5] in 1939 and also by Prandtl[6] in 1945. Prandtl[6] studied fully developed turbulence and pointed out that the state of turbulence at any given moment consists partly of a residual contribution from the previous flow history. Rotta[7] concluded from experimental data that, when turbulent flow is perturbed from its equilibrium state, it takes a distance about one order of magnitude greater than its boundary-layer thickness to attain a new equilibrium state. The so-called "zero-equation or algebraic eddy viscosity" turbulence model is derived based on the concept of an equilibrium turbulent boundary layer, depending only on the mean flow properties, and is incapable of conveying the upstream turbulence history. Nevertheless, current one- or two-equation models do not offer much improvement over the zero-equation models.[8] Meanwhile, more sophisticated models, such as Reynolds stress equations or subgrid scale turbulence models, are very costly in computation time, if not impractical. Therefore, the development of a modified simple algebraic eddy viscosity model for nonequilibrium flow which includes upstream history, if possible, is very attractive for solving the complete Navier-Stokes equations.

Shang and Hankey[9] used a relaxation eddy viscosity model to solve for supersonic flow over a compression corner. Their numerical reuslts, in comparison with Law's data,[10] indicated an improvement over Wilcox's[11] calculation, in which the two-equation differential Saffman turbulence model was used. Subsequently, Baldwin and Rose[12] and Shang et al.[13] also incorporated the relaxation model to simulate shock impingement problems and found results that were a significant improvement over those obtained with the simple eddy viscosity model. Recently, Deiwert[14] extended the relaxation model to simulate a transonic flow over a thick airfoil, and Mateer et al.[15] used a similar model to calculate a transonic normal shock-wave boundary-layer interaction. Even though the latter results qualitatively represent the interactive features, Mateer et al.[15] indicated some unfavorable effects in skin friction of applying the relaxation model.

It is the purpose of this paper to understand how the relaxation model works and to examine the applicability of the model for high Mach number flows with heat transfer. The end result hopefully will provide some information for further turbulence model development.

Analysis

Governing Equations

The viscous-inviscid interaction flowfield is governed by the time-dependent, compressible Navier-Stokes equations. Casting in terms of Reynolds mass-averaged variables, and with the bulk viscosity and the specific turbulent energy in the

Received June 28, 1976; presented as Paper 76-410 at the AIAA 9th Fluid and Plasma Dynamics Conference, San Diego, Calif., July 14-16, 1976; revision received Nov. 3, 1976.

Index categories: Boundary Layers and Convective Heat Transfer – Turbulent; Jets, Wakes, and Viscid-Inviscid Flow Interactions; Supersonic and Hypersonic Flow.

*Consultant, DCW Industries. Member AIAA.

†Assistant Chief, Computational Fluid Dynamics Branch. Member AIAA.

normal stress components omitted, the resulting mean conservative relations are the same as their laminar flow counterpart, except for the addition of the Reynolds stress tensor and the Reynolds heat flux. Turbulent closure is accomplished by expressing the Reynolds stress tensor in terms of the product of eddy viscosity ϵ with the mean velocity gradients. Also, turbulent Prandtl number Pr_t is used for the Reynolds heat flux. Thus, the mean flow equations in two dimensions can be written in integral form as

$$\frac{\partial}{\partial t}\int_{\text{volume}} U \text{ d vol} + \int_{\text{surface}} \vec{H}\cdot\vec{n}\,\text{d}S = 0 \tag{1}$$

where

$$U = \begin{bmatrix} \rho \\ \rho u \\ \rho v \\ E \end{bmatrix} \qquad \vec{H} = \begin{bmatrix} \rho\vec{q} \\ \rho u\vec{q} + \vec{\vec{\tau}}\cdot\vec{e}_x \\ \rho v\vec{q} + \vec{\vec{\tau}}\cdot\vec{e}_y \\ E\vec{q} + \vec{\vec{\tau}}\cdot\vec{q} + \vec{Q} \end{bmatrix}$$

$$\vec{q} = u\vec{e}_x + v\vec{e}_y$$

$$\vec{\vec{\tau}} = \sigma_x\vec{e}_x\vec{e}_x + \tau_{xy}\vec{e}_x\vec{e}_y + \tau_{yx}\vec{e}_y\vec{e}_x + \sigma_y\vec{e}_y\vec{e}_y$$

$$\sigma_x = p + \frac{2}{3}(\mu+\epsilon)\left(\frac{\partial u}{\partial x} + \frac{\partial v}{\partial y}\right) - 2(\mu+\epsilon)\frac{\partial u}{\partial x}$$

$$\tau_{xy} = \tau_{yx} = -(\mu+\epsilon)\left(\frac{\partial u}{\partial y} + \frac{\partial v}{\partial x}\right)$$

$$\sigma_y = p + \frac{2}{3}(\mu+\epsilon)\left(\frac{\partial u}{\partial x} + \frac{\partial v}{\partial y}\right) - 2(\mu+\epsilon)\frac{\partial v}{\partial y}$$

$$\vec{Q} = Q_x\vec{e}_x + Q_y\vec{e}_y$$

$$Q_x = -\left(\frac{\mu}{Pr} + \frac{\epsilon}{Pr_t}\right)\gamma\frac{\partial e}{\partial x}$$

$$Q_y = -\left(\frac{\mu}{Pr} + \frac{\epsilon}{Pr_t}\right)\gamma\frac{\partial e}{\partial y}$$

$$E = \rho[e + 0.5(u^2+v^2)]$$

and $\vec{e}_x$, $\vec{e}_y$ are unit vectors of the orthogonal (x,y) coordinate system, and $\vec{n}$ a unit normal vector of the surface enclosing the volume of integration. The equation of state relates the pressure p and density ρ to temperature T and specific internal energy e. The perfect gas relations are $p=\rho RT$ and $e=C_vT$. The molecular viscosity coefficient μ is assumed to be a function of temperature only and is evaluated by Sutherland's semiempirical formula $\mu = 2.270\times10^{-8}\ T^{3/2}/(T+198.6)$ (slug/ft-sec). In the present calculation, molecular Prandtl number Pr is assumed to be 0.72, and turbulent Prandtl number Pr_t is taken to be 0.90.

Computational Domain

Figure 1 shows the computation domain and the appropriate boundary conditions. The mesh is spaced equally in the x direction, but, in the y direction, a fine, geometrically stretched mesh spacing is used in the region near the wall ($y \le h_f$) for resolving the viscous layer, and a coarse, equally spaced mesh is used in the outer region ($h_f < y < h$), where viscous effects are negligible. The upstream boundary is located at a distance several boundary-layer thicknesses ahead of the interaction region defined from when the pressure starts to increase until it reaches its final value. The upstream conditions can be either generated from the present program by solving the Navier-Stokes equations over a flat plate that

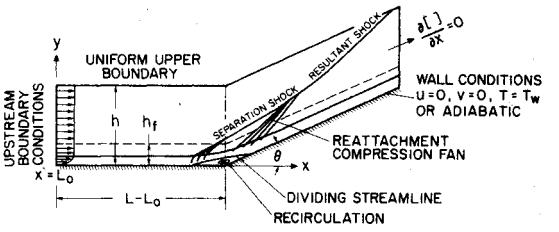

Fig. 1 Computational domain and boundary conditions.

includes leading edge effects, or supplied from conventional boundary-layer solution, such as Marvin and Shaeffer's code.[16] The downstream boundary is positioned far enough from the corner so that all of the gradients in the flow direction can be set at zero. Although this condition is not exact, the boundary layer in the vicinity of this exit is parabolic, and the remainder of the flow is supersonic; hence, it is not expected that this condition will introduce significant error in the region of interest upstream. The upper boundary is specified by the freestream conditions. The wall surface is assumed impermeable, and no-slip boundary conditions are applied. The wall is treated either as isothermal or adiabatic, and the wall pressure is evaluated from an approximation of the y-momentum equation at the wall. During the calculation of the inner mesh, transport and stress at the internal boundary, $y=h_f$, are saved, and their net quantities then are used as boundary conditions for the outer mesh flowfield.

The numerical method and special numerical procedures used in the calculation presented herein are described in detail in Refs. 2 and 3. The computer code was checked out initially for laminar flow cases to insure that the numerical scheme is accurate and efficient. (Details of laminar flow results were presented in Ref. 3) The same code is used herein to test the accuracy of turbulence models.

Eddy Viscosity Model

In the present study, a two-layer equilibrium eddy viscosity model ("equilibrium model") is applied in the following fashion. In the inner region, the Prandtl mixing length concept is used:

$$\epsilon_{\text{inner}} = \rho(KyD)^2[(\partial u/\partial y)^2 + (\partial v/\partial x)^2]^{1/2} \tag{2}$$

where K is von Karman's constant (0.4) and D van Driest's damping factor $D = 1-\exp[-y(|\tau_w|\rho)^{1/2}/26\mu]$. In the law of the wall for the outer region, the modified Cluser's defect law is employed:

$$\epsilon_{\text{outer}} = 0.0168\ \rho u_e \delta^* \beta \tag{3}$$

where β is the Klebenoff intermittency correction factor, $\beta = [1+5.5(y/\delta)^6]^{-1}$, u_e the velocity at the edge of the boundary layer, and δ^* the kinematic displacement thickness:

$$\delta^* = \int_{y_0}^{\delta}\left(1-\frac{u}{u_e}\right)\text{d}y$$

$$\delta = \text{minimum of } (\delta_1,\delta_2).\begin{cases}\delta_1 = y\,|\,[\max(\rho\mu),\ J<J_{\max}]\\ \delta_2 = y\,|\,[(\Delta u/u)<0.02]\end{cases}$$

y_0 is the location of zero velocity and $J_{\max}$ is a preassigned value, insuring that it is located outside of the boundary layer. Then the eddy viscosity is determined by

$$\epsilon_{eq} = \epsilon_{\text{inner}} \text{ of } y<y_i$$

$$= \epsilon_{\text{outer}} \text{ if } y>y_i \tag{4}$$

where y_i is the first point that $\epsilon_{\text{outer}} < \epsilon_{\text{inner}}$. A simple smoothing also is applied on δ^*.

Note that the local values of μ and ρ are used in D, as opposed to the more conventional format of using the wall values, a difference that might become significant in highly cooled or heated wall calculations. Use of y_0 as the lower bound for the integration of δ^* avoids picking up the unwanted negative (reverse) flow effects in evaluating the displacement thickness. The main difference of the presently employed equilibrium model from that used by Shang and Hankey[9] is that the velocity at the edge of boundary layer u_e (instead of the maximum velocity u_{max}) is used in the calculation of outer layer eddy viscosity ϵ_{outer} and the displacement thickness δ^*. Although it is difficult in viscous-inviscid interactions to determine the edge of the boundary layer, care should be taken to determine u_e. Without this effort, the maximum velocity, in general, will be the freestream velocity instead of the more typical boundary-layer edge velocity behind the induced shock. Use of the freestream velocity will overestimate δ^* and, in our experience, may cause up to a factor of 2 or more difference in the calculation of outer layer eddy viscosity ϵ_{outer}.

To account for the upstream turbulence history effects, Shang and Hankey[9] used a relaxation eddy viscosity model (herein designated "upstream relaxation"):

$$\epsilon = \epsilon_{eq} - (\epsilon_{eq} - \epsilon_0)\exp[-(x - x_0/\lambda)] \qquad (5)$$

where ϵ_0 = the eddy viscosity at upstream location x_0, and λ is the relaxation length. In concept, Eq. (5) approximates the experimental observation that, in an abrupt disturbance of a turbulent flow, the Reynolds stress remains nearly frozen at its initial value while it is being convected along streamlines, and then exponentially approaches a new equilibrium state. In a numerical calculation, the initial location of disturbance x_0, from which the relaxation process is initiated, and a relaxation length scale λ, which describes the exponential decay of the eddy viscosity distribution, need to be specified. The choice of x_0 and λ, although guided by observation, is still somewhat arbitrary. There are two limiting cases that bound the relaxation length. For $\lambda = 0$, the turbulent eddy viscosity equals the local equilibrium value, and for $\lambda = \infty$, the initial value ϵ_0 is frozen and is used everywhere in the region $x > x_0$.

Comparison and Discussion of Results

Supersonic Flow

The first case computed was for $M_\infty = 2.96$ supersonic flow over a 25° wedge with an adiabatic wall. The flow conditions correspond identically with one of the cases studied by Shang and Hankey[9] and with experimental data measured by Law[10]; these are given as follows: $M_\infty = 2.96$, $Re_L = 10^7$, $\alpha = 25°$, $T_\infty = 177°$R $L = 1$ ft, and adiabatic wall. The computational domain extends from $x/L = 0.795$ to $x/L = 1.205$, with the fine mesh boundary placed at $h_f = 0.025$ ft and the outer boundary at $h = 0.09$ ft. In the x direction, 63 mesh points are used, and in the y direction, a total of 31 mesh points are used, 20 for the fine mesh and 11 for the coarse mesh. The mesh spacing varies from $\Delta y)_{min} = 0.148 \times 10^{-3}$ ft to $\Delta y = 0.44 \times 10^{-2}$ ft for the fine mesh, and near the wall the mesh cells are very elongated with a ratio of $\Delta x{:}\Delta y)_{min} = 44{:}1$. For the case of interest, the compression is moderate (the pressure rise is about a factor of 5); the boundary-layer thickness is about the same before and after the interaction. Therefore, $\Delta y)_{min}$ is fine enough for use to insure that the first mesh points near the wall are in the sublayer ($y^+ < 10$) both upstream and downstream of the compression.

The upstream conditions are generated with the present numerical code by solving the flow over a flat plate with a leading edge. Figure 2 shows a u-velocity profile compared with a boundary-layer solution[16] and Shang and Hankey's result.[9] The agreement is very good. Plotted on the non-

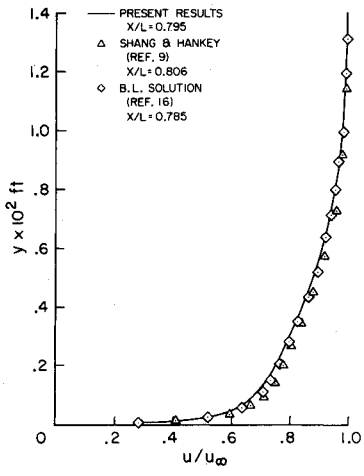

Fig. 2 Flat-plate solution. $M_\infty = 2.96$; $Re_L = 10^7$.

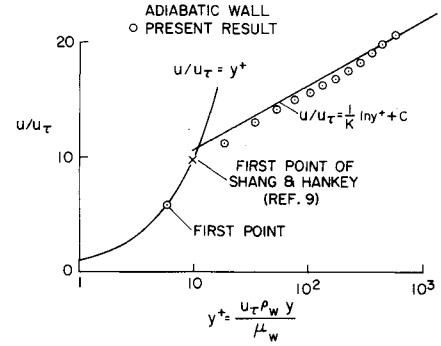

Fig. 3 Law of the wall. $M_\infty = 2.96$; $x/L = 0.795$; $Re_L = 10^7$.

dimensional scale of (u/u_τ) vs y^+, the profile is in surprisingly good agreement with the law of the wall (Fig. 3). The value of y^+ of the first mesh point of the present study is about 5.8, and that of Ref. 9 is just under 10. Figures 4a and 4b show comparisons of pressure and skin friction ($c_f = 2\tau_w/\rho_\infty u_\infty$) calculated using the present equilibrium model with the experimental measurements of Law.[10] The equilibrium model tends to overpredict the surface pressure in the reattachment and downstream regions and underpredicts the upstream pressure rise and, thus, the location of the separation point. Also shown in these two figures is a comparison of the equilibrium results of Ref. 9 with those of the present study. Even with the good agreement found upstream (Fig. 2), the results here are substantially different because of the difference in formulating the eddy viscosity models. The use of u_{max} instead of u_e in Ref. 9 tends to provide a higher eddy viscosity and thus more mixing inside the boundary layer, which makes it more resistant to separation. The modeling difference is relatively insensitive in the flat-plate solution, even though the boundary-layer profile in Ref. 9 does show slighly more momentum from the increased mixing. In the interaction region where a shock wave lies above the boundary layer, it causes a significant difference.

Using the upstream relaxation model, good improvement in predictions of upstream pressure rise is obtained, and a more pronounced pressure plateau region clearly is demonstrated (Figs. 5a and 5b). For the present supersonic case, the relaxation length is chosen about $\lambda = 5\ \delta_0$, where δ_0 is the boundary-layer thickness at $x = x_0$, and the initial location is positioned at $x_0/L = 0.9387$. Shown in the figures also are the results of equilibrium and frozen cases, which bound the effect of changing the relaxation length scale from $\lambda = 0$ to $\lambda = \infty$. In Fig. 6, the calculated density contours, obtained by using the relaxation model, are compared with the interferogram and a schematic of the experimental flowfield in Ref. 17. The details of the interaction pattern, including

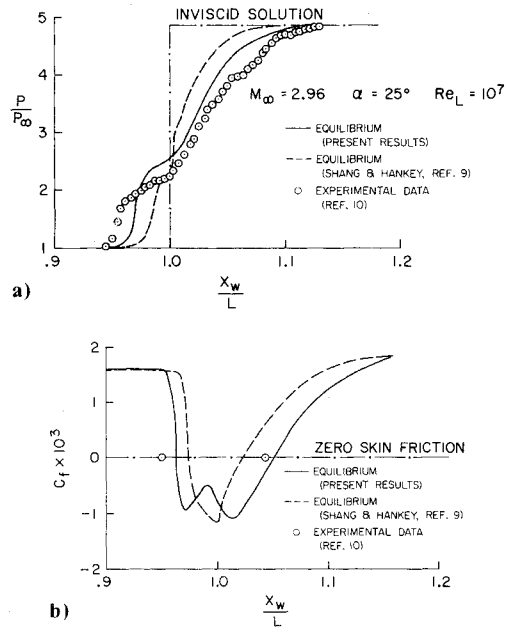

Fig. 4 Comparison of the results of equilibrium models. a) Surface pressure. b) Skin friction.

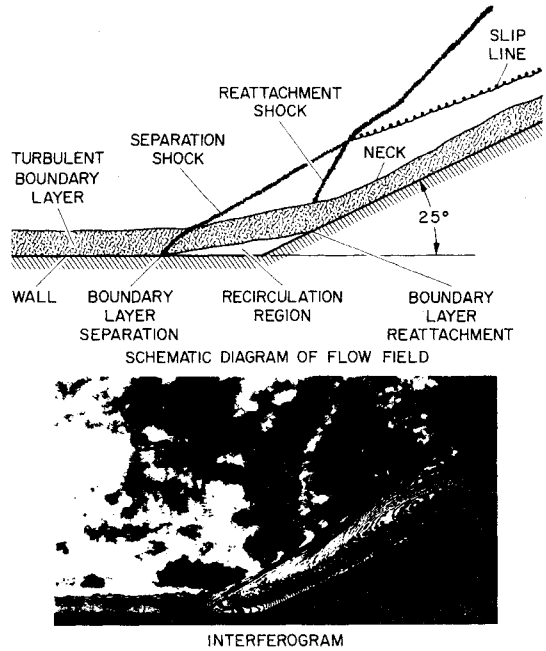

INTERFEROGRAM

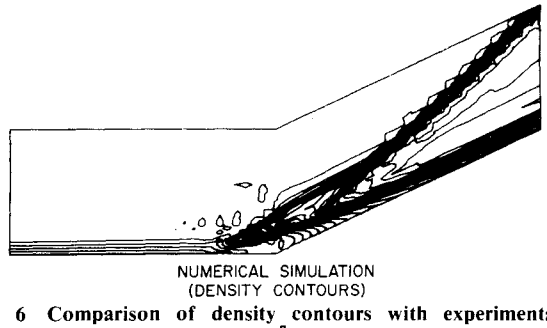

NUMERICAL SIMULATION (DENSITY CONTOURS)

Fig. 6 Comparison of density contours with experimental interferogram. $M_\infty = 2.96$; $Re_L = 10^7$; $\alpha = 25°$.

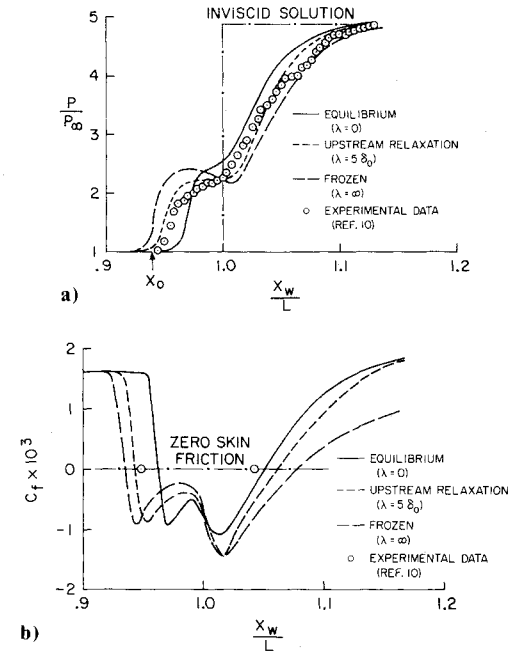

Fig. 5 Results of different relaxation lengths. a) Surface pressure. b) Skin friction. $M_{1/2} = 2.96$; $\alpha = 25°$; $Re_L = 10^7$; $\delta = 0.01403$ ft; $x_0/L = 0.9387$.

separation shock, separation, and reattachment shock, are shown to be well simulated.

Since the inclusion of relaxation effects results in improved comparisons of theory with experiment, it is important to understand how the relaxation model works. Figure 7 shows the variation of eddy viscosity at five levels from the wall, with the relaxation length $\lambda = 5\ \delta_0$. The symbols represent the values evaluated from local equilibrium model ϵ_{eq}, and the lines are the turbulent dynamic eddy viscosity, which is based on the upstream relaxation formula, Eq. (5). The first three sets of data (lines and symbols) for the smaller values of y belong to the inner layer of the eddy viscosity model, the data for $y/\delta_0 = 0.0928$ are taken near the location of the transition from the inner to outer layers, and the outermost y-level data are calculated from the outer layer formula, Eq. (3). Near the wall (circle symbol, Fig. 7), the eddy viscosity is small, $\epsilon_{eq} < \mu_w$, and is dominated greatly by the wall shear stress and the local velocity gradient [see Eq. (2)]. At the beginning of the interaction, ϵ_{eq} near the wall decreases sharply because of the decrease of τ_w, reaching a minimum at separation. The minimum of ϵ_{eq} appears again at the point of reattachment. Note that $\tau_w = 0$ at the separation and reattachment points, and thus, from Eq. (2), $D = 0$ and $\epsilon_{inner} = 0$. Therefore, based on the local equilibrium model, Eqs. (2-4), there is no eddy viscosity, whereas in the real flow, turbulence fluctuations do exist at separation and reattachment. The application of the upstream relaxation process greatly increases the eddy viscosity values in these regions and only slightly affects the values in the downstream region when x/L is large.

In contrast to the effect at small y, ϵ_{eq} increases sharply at large y because of the increase in $\rho\delta^*$ resulting from the compression of the separation shock. The relaxation process drastically modifies the increasing slope and provides values of ϵ substantially less than that of the equilibrium model. The effects of the relaxation process can be examined more clearly in Fig. 8, in which eddy viscosity profiles at three x locations are plotted across the boundary layer. The reduction of eddy viscosity from its local equilibrium value far from the wall leads to less turbulence mixing and to less shear stress to balance the adverse pressure gradient, making the separation easier and allowing better upstream pressure rise through the viscous and inviscid interaction.

It is interesting to recall the result of the frozen case ($\lambda = \infty$) in which initial value ϵ_0 is used everywhere downstream of $x > x_0$. This causes the eddy viscosity in the outer region to be

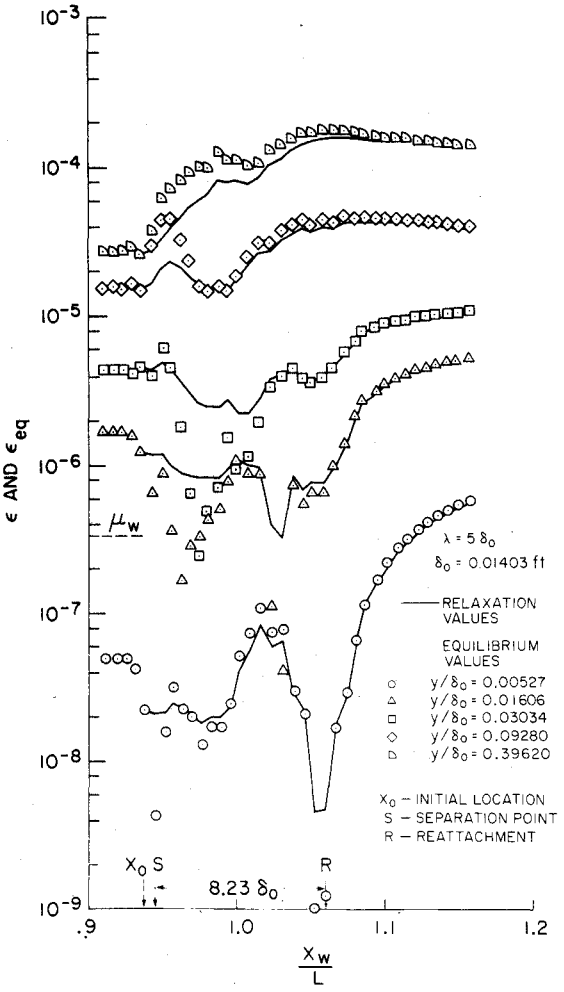

Fig. 7 Eddy viscosity at five y levels with upstream relaxation.

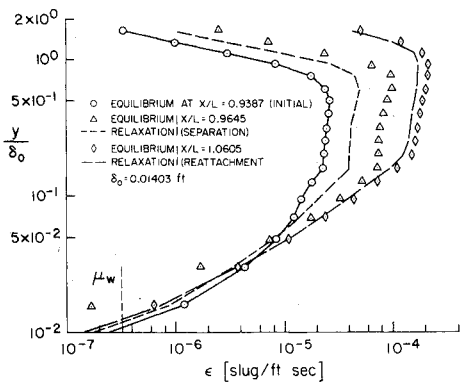

Fig. 8 Eddy viscosity at three x locations.

reduced by about a factor of 6 and near the wall by about a factor of 10, below the equilibrium value in the downstream region (see Fig. 7 curves of $y/\delta_0 = 0.00527$ and $y/\delta_0 = 0.3962$). Hence, although the surface pressure closely reaches the value of the inviscid solution, the skin friction is about a factor of 2 under the equilibrium result (see Fig. 5b).

To summarize the supersonic flow case, it was found out that the local equilibrium formula overpredicts the value of eddy viscosity, at least at the region right after the separation pressure rise. In general, the relaxation process reduces the eddy viscosity value in the outer layer of the separation region and shows substantial improvement in predicting the upstream pressure propagation. Relaxation models tend to locate the reattachment point downstream of the experimental result. This might be an indication of an underprediction of

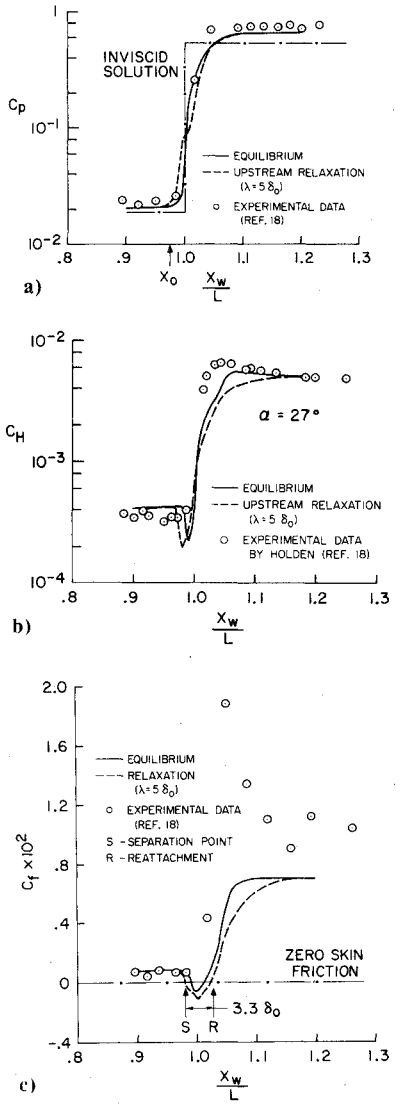

Fig. 9 Comparisons of the results of equilibrium and relaxation models with experiments for $M_\infty = 8.66$ and $\alpha = 27°$. a) Pressure coefficient; b) Heat transfer. c) Skin friction. $M_\infty = 8.66$; $\alpha = 27°$; $Re_L = 2.2 \times 10^7$; $L = 2.25$ ft; $\delta_0 = 0.0323$ ft; $x_0/L = 0.9762$.

eddy viscosity in the reattachment region. Surface pressure seems insensitive to different turbulence models in the downstream region. Further study should be made based on more detailed comparisons of experimental flowfield and skin-friction measurements.

Hypersonic Flows

At hypersonic speeds, compressibility makes drastic changes in the nature of turbulent flow. The turbulence disturbances are composed mostly of density and temperature fluctuations. At high hypersonic speeds, a slight local velocity change in the fluid would cause a large change in its temperature. Therefore, one might expect the test of turbulence model accuracy to be more severe in this case. As we recall, the simple equilibrium eddy viscosity model was derived originally based on the turbulent velocity fluctuations of incompressible flow. The purpose of this section is to investigate how the simple eddy viscosity model with relaxation behaves at high Mach numbers with heat transfer.

The experiments selected for comparison were conducted by Holden,[18] and measurements were made of pressure, skin friction, and heat transfer along the wall. The flow conditions are as follows: $M_\infty = 8.66$, $Re_L = 2.2 \times 10^7$, $T_w = 537°$R, $T_\infty = 119.5°$R, $L = 2.25$ ft, and $\alpha = 27°$ and $36°$. The wall is

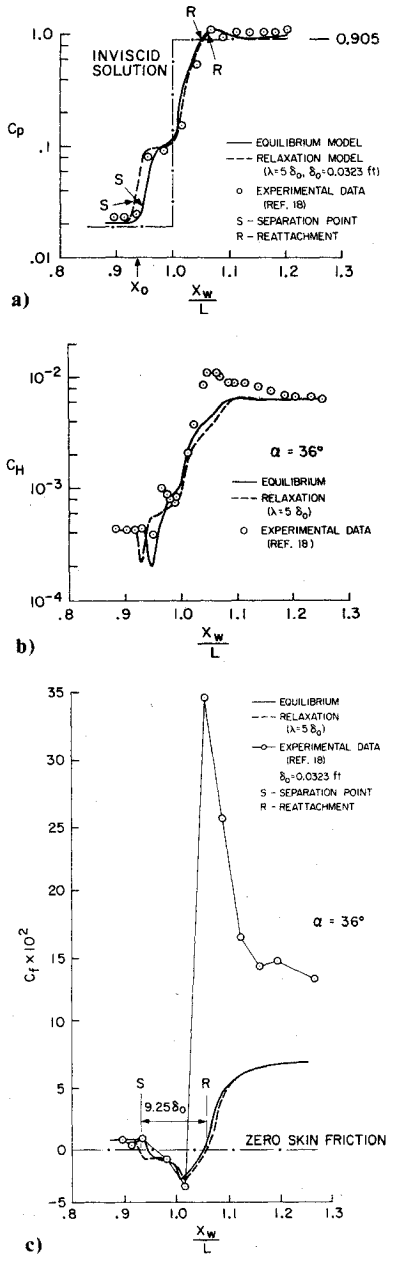

Fig. 10 Comparisons of the results of equilibrium and relaxation models with experiments for $\alpha = 36°$. a) Wall pressure. b) Heat-transfer coefficient. c) Skin friction at $\alpha = 36°$.

assumed to be isothermal and highly cooled. The ratio of wall temperature to adiabatic temperature is about $T_w/T_{aw} = 0.28$. As in the previous supersonic problem, a mesh with 63 points in the x direction and 31 in the y direction is used. Now, however, the fine mesh contains 21 points for better resolution. The upstream boundary is located at $x/L = 0.881$, with 23 points of equal space resolution between the upstream boundary and the hinge line of the wedge, which is at $x/L = 1.0$. The mesh cells near the wall are very elongated, with $\Delta x/\Delta y_{\min} = 226$. the computation is advanced about 95 times in the inner mesh loop for every outer mesh time step.

Figures 9 and 10 show the detailed comparisons of the present calculated results with the experimental measurements of surface pressure, heat transfer, and skin friction for $\alpha = 27°$ and $36°$. The pressure coefficient is defined as $c_p = 2p_{\text{wall}}/\rho_\infty u_\infty^2$ and the heat transfer coefficient as $c_H = k(\partial T/\partial y)\sec\theta/\rho_\infty u_\infty \{[e + (p/\rho) + u^2/2]_\infty - [e + (p/\rho)]_w\}$. The agreement is very good upstream of the interaction region. This implies that, at least in this study, the equilibrium eddy viscosity model can be used to predict equilibrium

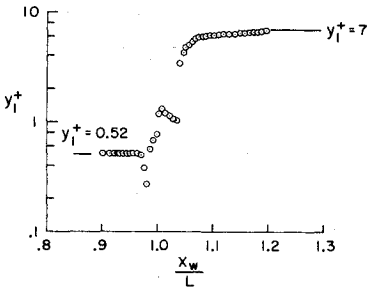

Fig. 11 y^+ of the first mesh points only x direction for $\alpha = 27°$ (relaxation model). $\alpha = 27°$; relaxation $(\lambda = 5\delta_0)$. $M_\infty = 8.66$; $\alpha = 36°$; $Re_L = 2.2 \times 10^7$; $T_w = 537°R$; $L = 27$ in.; $x_0/L = 0.9392$.

hypersonic turbulent flow over a flat plate. The fluctuations of temperature and density may be considered as a simple function of the fluctuation of velocity, and the simple eddy viscosity relation does provide proper turbulence mixing in the equilibrium hypersonic turbulent boundary layer. Surprisingly enough, the results also show reasonably good agreement in surface pressure and heat transfer in the interaction region, although the peak heat transfer at the reattachment point is underpredicted. The present heat transfer results are significantly different from that of the laminar flow case studied.[3] Instead of very low heat transfer in the separation region as in the laminar case, the heat transfer here drops sharply near the separation point, rises rapidly to a value greater than its upstream condition, gradually increases in the pressure plateau region, and then sharply increases under strong compression. As the separation region becomes larger, a heat-transfer plateau region forms, similar to that of the surface pressure. In experimental measurements, heat transfer does not show a sharp decrease at separation, and, instead of the slow gradual increase, it indeed shows a slight decrease in the pressure plateau region. It still is not clear whether the sharp, deep drop of heat transfer near the separation point is physically correct or is caused by the shortcomings of the simple eddy viscosity model. As we pointed out in the supersonic case (Fig. 7), the eddy viscosity model tends to provide a very low value of eddy viscosity near the wall at separation point. The underprediction of peak heat transfer in the reattachment region also might be caused by the same shortcoming of the turbulence model.

Unfortunately, even though the points of separation and reattachment are predicted reasonably, the skin friction is underpredicted grossly in the regions of reattachment and downstream recompression. This strongly suggests that the value of eddy viscosity for the present hypersonic case is underpredicted in these highly compressed regions. From the experience of the previous frozen case result, it may be suspected that the eddy viscosity value is several times below that of the real experimental flowfield.

The application of the upstream relaxation process, also shown in Figs. 9 and 10, does show increasing upstream pressure propagation. However, it also shows unfavorable effects of decreasing skin friction and heat transfer after reattachment, especially in the results of the $\alpha = 27°$ case, in which the separation region is small and the initial location x_0 is positioned very close to reattachment. This may confirm our previous argument that the simple equilibrium eddy viscosity model underpredicts the eddy viscosity value in the reattachment and downstream recompression regions, and, moreover, the relaxation process reduces the eddy viscosity value still further. The current eddy viscosity model, with or without the inclusion of relaxation, fails to simulate sharp peaks of heat transfer and skin friction in the neck region right after reattachment in the cold-wall hypersonic case. For future turbulence modeling, special attention should be focused on what is required to obtain sharp peak skin friction and heat transfer in the neck region.

One interesting aspect of the strong compression associated with the hypersonic problem is the severe restriction imposed on $\Delta y)_{\min}$ along the wall. As shown in Figs. 9a and 10a, the pressure rises by a factor of about 30 for the case of $\alpha = 27°$ and about 50 for $\alpha = 36°$. The thickness of the boundary layer after compression is one order of magnitude thinner than that before the interaction. To insure enough mesh resolution in the downstream highly compressed region, $\Delta y)_{\min}$ for the first mesh cell has to be very small. Figure 11 shows a plot of y^+ at the first mesh point vs x. At the upstream region, y_1^+ is far inside the sublayer ($y_1^+ \approx 0.52$), stays small in the separation region, and sharply increases right after the reattachment up to about 7. One should bear in mind that the present y_1^+ is evaluated based on the computed skin friction. For instance, if these values are calculated with the experimental skin friction, y_1^+ would increase by a factor of $[\tau_w(\text{experiment})/\tau_w(\text{calculated})]^{1/2} \approx (2)^{1/2}$ for $\alpha = 27°$ case, which may result in a $y_1^+ \approx 10$ in the downstream region. However, y_1^+ is small in the separation region, and the boundary layer in the downstream region is parabolic; hence, a y_1^+ of about 10 in the downstream region should underpredict primarily only the local skin friction and would not be expected to introduce significant error in the separation region.

Conclusions

Supersonic and hypersonic turbulent flows over a two-dimensional compressional corner have been simulated numerically. The complete time-dependent Reynolds mass-averaged Navier-Stokes equations with equilibrium and relaxation eddy viscosity models were solved. Computed solutions were compared with the experimental measurement of Law[10] for supersonic flow and of Holden[16] for hypersonic flow. Details of the relaxation process were studied. In general, the equilibrium model predicts a sharp increase of outer-layer eddy viscosity near the separation pressure rise, whereas the relaxation process substantially decreases the eddy viscosity value and predicts better upstream pressure propagation. The simple eddy viscosity model indeed predicts, with very good agreement, upstream boundary conditions in the hypersonic boundary layer. However, it significantly underpredicts the value of eddy viscosity and, hence, the level of skin friction in the reattachment and downstream recompression regions. The application of relaxation process reduces the eddy viscosity value further and shows unfavorable effects on heat transfer and skin friction for hypersonic flow in these regions.

References

[1] Peyret, R. and Viviand, H., "Computation of Viscous Compressible Flows Based on the Navier-Stokes Equations," AGARDograph 212, Sept. 1975.

[2] MacCormack, R. W. and Baldwin, B. S., "A Numerical Method for Solving the Navier-Stokes Equations with Application to Shock-Boundary Layer Interactions," AIAA Paper 75-1, Pasadena, Calif., 1975.

[3] Hung, C. M. and MacCormack, R. W., "Numerical Solutions of Supersonic and Hypersonic Laminar Flows over a Two-Dimensional Compression Corner," *AIAA Journal*, Vol. 14, April 1976, pp. 475-481.

[4] Carter, J. E., "Numerical Solutions of the Navier-Stokes Equations for Supersonic Laminar Flow over a Two-Dimensional Compression Corner," NASA TR R-385, July 1972.

[5] Jacobs, W., "Umformung eines turbulenten Geschwindigkeitsprofiles," *Zeitschrift fur Angewandte Mathematik und Mechanik*, Vol. 19, April 1939, pp. 87-100.

[6] Prandtl, L., "On a New Representation of Fully Developed Turbulence," transl. by D. Coles, Jet Propulsion Lab., Pasadena, Calif., Publication No. 13, 1952.

[7] Rotta, J. C., "Turbulent Boundary Layers in Incompressible Flow," *Progress in Aerospace Sciences*, Vol. 2, Pergamon Press, New York, 1962, pp. 1-220.

[8] Baldwin, B. S. and MacCormack, R. W., "Interaction of Strong Shock Wave with Turbulent Boundary Layer," AIAA Paper 74-558, Palo Alto, Calif., 1974.

[9] Shang, J. S. and Hankey, W. L., "Numerical Solution of the Navier-Stokes Equations for Compression Ramp," *AIAA Journal*, Vol. 13, Oct. 1975, pp. 1368-1374, (supplemental data included in private communication).

[10] Law, C. H., "Supersonic Turbulent Boundary-Layer Separation," *AIAA Journal*, Vol. 12, June 1974, pp. 794-797.

[11] Wilcox, D. C., "Numerical Study of Separated Turbulent Flows," *AIAA Journal*, Vol. 13, May 1975, pp. 555-556.

[12] Baldwin, B. S. and Rose, W. C., "Calcualtion of Shock-Separated Turbulent Boundary Layers," *Proceedings of the NASA Conference on Aerodynamic Analysis Requiring Advanced Computer*, NASA SP-347, March 1975.

[13] Shang, J. S., Hankey, W. L., and Law, C. H., "Numerical Simulation of Shock Wave-Turbulent Boundary-Layer Interaction," *AIAA Journal*, Vol. 14, Oct. 1976, pp. 1451-1457.

[14] Deiwert, G. S., "Computation of Separated Transonic Turbulent Flows," *AIAA Journal*, Vol. 14, June 1975, pp. 735-740.

[15] Mateer, G. G., Brosh, A., and Viegas, J. R., "A Normal Shock-Wave Turbulent Boundary-Layer Interaction at Transonic Speeds," AIAA Paper 76-161, Washington, D.C., 1976.

[16] Marvin, J. G. and Sheaffer, Y. S., "A Method for Solving the Nonsimilar Laminar Boundary-Layer Equations Including Foreign Gas Injection," NASA TN D-5516, Nov. 1969.

[17] Havener, A. G. and Radley, R. J., "Supersonic Wind Tunnel Investigations Using Pulsed Laser Holography," Aerospace Research Lab., Wright-Patterson Air ForceBase, Ohio. ARL 73-0148, Oct. 1973.

[18] Holden, M. S., "Shock Wave-Turbulent Boundary Layer Interaction in Hypersonic Flow," AIAA Paper 72-74, San Diego, Calif., 1972, (supplemental data included in private communication).